

Static over-the-barrier model for electron transfer between metallic spherical objects

H. Zettergren, H. T. Schmidt, and H. Cederquist

Physics Department, Stockholm University, SCFAB, S-106 91 Stockholm, Sweden

J. Jensen

Manne Siegbahn Laboratory, Frescativägen 24, S-104 05 Stockholm, Sweden

S. Tomita and P. Hvelplund

Institute of Physics and Astronomy, University of Aarhus, DK-8000, Århus C, Denmark

H. Lebius and B. A. Huber

CIRIL/GANIL, rue Claude Bloch, BP 5133, 14070 Caen Cedex 5, France

(Received 26 November 2001; revised manuscript received 10 May 2002; published 19 September 2002)

We present a *static* classical over-the-barrier model (OBM) for electron transfer between two isolated, infinitely conducting spheres with arbitrary and different electrical charges. This model is shown to be very useful for first estimates of single- and multiple-electron transfer cross sections in cluster-cluster collisions when the collision velocities are significantly lower than the typical target electron velocities. For faster collisions, more advanced models such as the dynamical OBM, or the time-dependent local density approximation (TDLDA) or the solutions of their semiclassical counterparts—the Vlasov equations have to be used. The latter two methods clearly provide the most detailed information on the electronic response, but they are also computationally very demanding and have, so far, only been used for collisions involving one cluster (and an atomic ion). We compare our static OBM results (in the limit in which one of the sphere radii approaches zero) with TDLDA and Vlasov calculations of cluster charging in $\text{Ar}^{8+}\text{-Na}_{40}$ collisions at different velocities to demonstrate that the present static OBM is valid at sufficiently low velocities. The static OBM is then used in a comparison with experimental target charge state distributions in $\text{C}_{60}^{q+}\text{-C}_{60}$ and $\text{C}^{q+}\text{-C}_{60}$ collisions at $0.01\sqrt{q}$ and $0.06\sqrt{q}v_0$, respectively. Calculated electronic excitation of the projectile after two-electron transfer in $\text{C}_{60}^{4+}\text{-C}_{60}$ collisions readily explains the recently observed suppression of the transfer ionization channel in this reaction. Finally, we model the total projectile electron loss and dissociation cross section in highly protonated Lysozyme-oxygen ($\text{Lys-H}_9^{9+}\text{-O}_2$) collisions and make comparisons with recent experimental results at $0.01v_0$.

DOI: 10.1103/PhysRevA.66.032710

PACS number(s): 34.70.+e

I. INTRODUCTION

Following Ryufuku *et al.* [1], Bárány *et al.* [2] and Niehaus [3] developed the first over-the-barrier models (OBM's) for *multiple* charge transfer in slow ion-atom collisions in 1985 and 1986. These models have turned out to be extremely useful for estimates of the total and absolute cross sections for electron removal from an atomic target. The atomic models [2,3] assume that electron transfer is possible when the over-the-barrier condition is fulfilled, i.e., when the potential seen by the electron moving from the target to the projectile equals the Stark-shifted binding energy for the active electron at the target. In 1991 Burgdörfer *et al.* [4] presented a similar model for ion-metal surface collisions in which the potential barrier was deduced from the quantum image charges, the active electron, and the ion itself. An extension of the latter model, valid also for insulator surfaces, was presented by Hägg *et al.* [5] in 1997. These ion-surface OBM's are dynamic in the sense that they take the time available for the active electrons to flow over the saddle point of the barrier into account. Similar ideas were applied for slow collisions between highly charged ions and clusters, describing electron transfer in a dynamical OBM, by Thumm *et al.* [6].

The time-dependent local-density approximation (TDLDA) has been applied to $\text{Ar}^{8+}\text{-C}_{60}$, $\text{Ar}^{8+}\text{-Na}_{40}$, and $\text{Ar}^{8+}\text{-Na}_{196}$ collisions [7]. This quantum-mechanical method gives very detailed information on the electronic response of the cluster including the time evolution of the electronic density distributions which, for instance, means that the emission of electrons during the collision process itself may be traced. It has been shown that the semiclassical counterpart of such TDLDA calculations, which involves the solving of the Vlasov equations [8], gives a charging of the cluster as a function of impact parameter in close agreement with those for the TDLDA [9]. Even more advanced calculations in which the motions of both the electrons and the heavy particles are followed have been performed by Knospe and co-workers, who used nonadiabatic quantum molecular dynamics (NA-QMD) to calculate charge transfer and fragmentation in, e.g., 2.7-keV $\text{Na}_4^+\text{-Cs}$ collisions [10]. These methods (TDLA, Vlasov, NA-QMD) are, however, computationally very demanding, and so far no results for which both collision partners are clusters have been presented. The virtue of the present static OBM model for cluster-cluster collisions is its great simplicity through which one can easily get first estimates of charge-exchange cross sections and electronic excitations of the cluster projectile

after the collision as we will show in detail below.

The first experiment with highly charged ions and C_{60} -molecules was performed in 1994 by Walch *et al.* [11], and they used a simple static OBM (treating C_{60} as a metal sphere) in order to interpret their results on relative cross sections for removing r electrons from C_{60} in slow Ar^{8+} - C_{60} collisions. This pioneering experiment was followed by ranges of other studies involving, e.g., charge transfer between C_{60} molecules [12,13], precision projectile energy gain measurements [14], projectile angular differential measurements [15,16] and thermionic emission from hot C_{60}^- [17]. Nowadays, the most advanced experiments involve multiple coincidence measurements between projectile scattering, target ionization, fragmentation and electron emission statistics [18]. Additional efforts are made to extract information on kinetic-energy releases, sequencing of C_{60} fragmentation cascades [19], and energy-transfer mechanisms [20,21]. In parallel, advances with static and dynamic over-the-barrier models describing electron transfer, projectile scattering, and energy gain for atomic-ion C_{60} interactions have been made [6,15,16,22,23].

In Sec. II, we present the static model describing over-the-barrier electron transfer between two (infinitely conducting) metal spheres. For completeness, we first follow Näher *et al.* [24] and show the solution for the electrostatic potential on a line connecting the centers of two charged spheres (sec. II A). In Sec. II B, we arrive at the exact expression for the potential experienced by an electron moving between the two spheres, taking the additional polarizations induced in the spheres by the active electron into account. Section II C deals with the over-the-barrier condition, i.e., the problem of finding the critical distances at which the Stark-shifted target electrons become free to move to the projectile sphere. In this section, we also give an expression for the electronic excitation of the projectile following single- and multiple-electron transfer. In Sec. II D, we show that the model reduces to the classical over-the-barrier models for (atomic) ion-sphere and ion-atom collisions when only the projectile radius and both radii are set to zero, respectively. In Sec. III A, we first consider one of these limiting cases to argue that it will be sufficient to use a *static* OBM for sufficiently low velocities in collisions between the highly charged ions and the Na clusters. This result is inferred from a comparison of the present static OBM results with TDLDA and semiclassical results using the Vlasov equations for the cluster charging as a function of the impact parameter in 80- and 320-keV Ar^{8+} - Na_{40} collisions. In Sec. III B, we are then able to compare the static OBM results to experimental recoil ion charge state fractions for much slower C_{60}^{q+} - C_{60} and C^{q+} - C_{60} collisions [25]. The model excitation energies in C_{60}^{4+} - C_{60} collisions at $v=0.024 v_0$ are calculated in Sec. III C and these results are used to rationalize the observation of the complete suppression of the transfer ionization channel in processes with two active electrons [26]. Finally, we use the static OBM to explain the observation of electron *loss* in highly protonated $Lys-H_9^{9+} + O_2$ collisions at very low velocities, which was recently reported by Hvelplund *et al.* [27]. In the

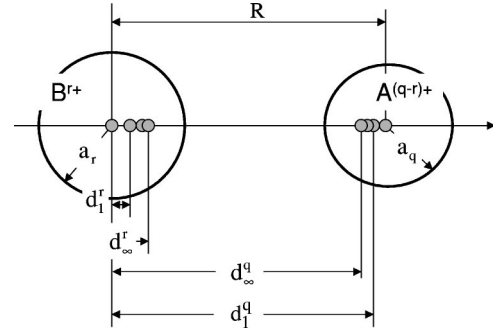


FIG. 1. The positions d_n^r and d_n^q (relative to the target center) of the image charges induced in the target B^{r+} and the projectile $A^{(q-r)+}$, respectively.

following sections, we will use atomic units unless otherwise stated.

II. THE MODEL

A. Two isolated metal spheres

The polarization of a *single* metal sphere in the presence of a point charge can be described by means of only two image charges [28], one at the sphere center and one at a position given by the position of the point charge and the radius of the sphere. However, two infinite sets of image charges are required (one in each sphere) in order to describe the polarization in the (charged) *sphere-sphere problem* exactly [24,29]. Here, we are aiming at the description of sequential transfer of an arbitrary number (r) of electrons from a spherical target to a spherical projectile (treated in Secs. II B and II C). Therefore, we start by treating the pure sphere-sphere problem and assign arbitrary net charges r and $q-r$ (and sphere radii a_r and a_q), to the target (B) and projectile (A) spheres, respectively. The positions of the target and projectile image charges, d_n^r and d_n^q , relative to the position of the target sphere center ($d_0^r=0$) are given by

$$d_{n+1}^r = a_r^2 / d_n^q,$$

$$d_{n+1}^q = R - a_q^2 / (R - d_n^r), \quad (1)$$

where the center position of the projectile sphere is $d_0^q=R$. The positions of the image charges converge towards d_∞^r and d_∞^q when $n \rightarrow \infty$ as indicated schematically in Fig. 1. From Eq. (1), we deduce expressions for the positions d_∞^r and d_∞^q ,

$$(d_\infty^r)^2 - (R^2 - a_q^2 + a_r^2) d_\infty^r / R + a_r^2 = 0,$$

$$(d_\infty^q)^2 - (R^2 - a_q^2 + a_r^2) d_\infty^q / R + a_r^2 = 0, \quad (2)$$

with solutions inside the target ($0 \leq d_\infty^r \leq a_r$) and the projectile ($R - a_q \leq d_\infty^q \leq R$) spheres. The corresponding absolute magnitudes of the target and projectile image charges, r_n and q_n , are

$$\begin{aligned} r_{n+1} &= -q_n a_r / d_n^q, \\ q_{n+1} &= -r_n a_q / (R - d_n^r). \end{aligned} \quad (3)$$

Note that r_n and q_n are well defined in terms of the center charges r_0 and q_0 . These, in turn, are given by charge conservation (charge transfer is treated in following sections)

$$\begin{aligned} r &= \sum_{n=0}^{\infty} r_n, \\ q - r &= \sum_{n=0}^{\infty} q_n. \end{aligned} \quad (4)$$

The expressions (1), (3), and (4) yield the exact solutions for the polarizations of both spheres. In order to be able to express r_0 and q_0 in terms of r and $q - r$ more clearly, Eq. (3) is rewritten as

$$\begin{aligned} r_{2n-1} &= \lambda_{2n-1} q_0, \\ r_{2n} &= \lambda_{2n} r_0, \\ q_{2n-1} &= \mu_{2n-1} r_0, \\ q_{2n} &= \mu_{2n} q_0. \end{aligned} \quad (5)$$

The coefficients λ_n and μ_n with odd n are the ratios between the strengths of the induced image charge and the center charge in the opposite sphere, while λ_n and μ_n with even n give the strengths of the induced image charges in relations to the center charge in the same sphere. The explicit values of λ_n and μ_n are then obtained by combining Eq. (3) and Eq. (5):

$$\begin{aligned} \lambda_{2n} &= \prod_{i=0}^{n-1} \frac{-a_q}{(R - d_{2i+1}^r)} \prod_{i=0}^{n-1} \frac{-a_r}{d_{2i+1}^q}, \\ \lambda_{2n+1} &= \prod_{i=0}^{n-1} \frac{-a_q}{(R - d_{2i+1}^r)} \prod_{i=0}^n \frac{-a_r}{d_{2i}^q}, \\ \mu_{2n} &= \prod_{i=0}^{n-1} \frac{-a_q}{(R - d_{2i+1}^r)} \prod_{i=0}^{n-1} \frac{-a_r}{d_{2i}^q}, \\ \mu_{2n+1} &= \prod_{i=0}^n \frac{-a_q}{(R - d_{2i+1}^r)} \prod_{i=0}^{n-1} \frac{-a_r}{d_{2i+1}^q}. \end{aligned} \quad (6)$$

The absolute magnitudes are smaller than unity for all n ($0 < |\lambda_n| < 1$ and $0 < |\mu_n| < 1$), since $a_q < R - d_n^r$ and $a_r < d_n^q$. Figure 2 (left part) shows $|\lambda_n|$ and $|\mu_n|$ as functions of n , for example where $a_r = a_q = 7.2 a_0$ and $R = 15, 25, 35 a_0$. These are typical values for interactions between two atomic clusters (as e.g., C_{60}). For fixed values of R and n and equal sphere radii ($a_q = a_r$), $|\lambda_n|$ and $|\mu_n|$ are equal and decrease exponentially with increasing n . For decreasing center-center distances (R), the polarization effect becomes larger and $|\lambda_n|$ and $|\mu_n|$ decrease less rapidly with n . In Fig. 2 (right

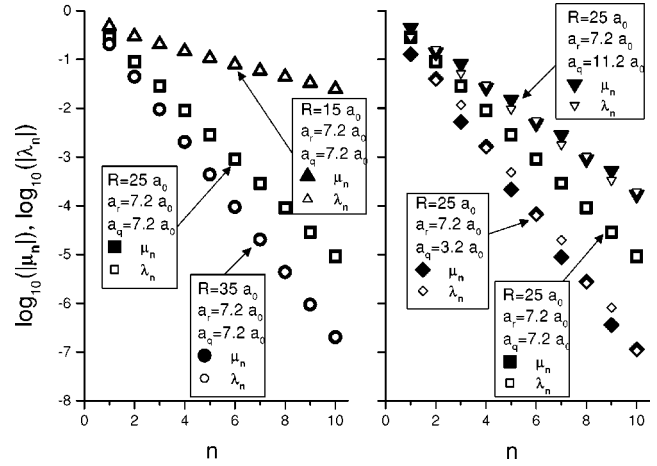


FIG. 2. Absolute values of λ_n and μ_n as functions of n for $a_r = a_q = 7.2 a_0$ and different center-center distances R (left figure). $|\lambda_n|$ and $|\mu_n|$ as functions of n at a constant center-center distance $R = 25 a_0$, a fixed value $a_r = 7.2 a_0$ and different values of a_q (right figure).

part), we show results for $R = 25 a_0$, $a_r = 7.2 a_0$, and $a_q = 3.2, 7.2, 11.2 a_0$. Note that $|\lambda_n|$ and $|\mu_n|$ do not coincide as in the left figure due to the different radii of the spheres. With decreasing a_q , which correspond to larger sphere surface-surface distances, $|\lambda_n|$ and $|\mu_n|$ decrease more rapidly. The relative magnitudes of $|\lambda_n|$ and $|\mu_n|$ as functions of n in these different situations directly give the relative strengths of the different multipole terms describing the full polarizations of the two spheres. The total charge of each sphere is conserved [Eq. (4)] giving the following expressions for the center charges as functions of the target and projectile net charges [$r_0 = r_0(q - r, r)$ and $q_0 = q_0(q - r, r)$]

$$\begin{aligned} r_0 &= \left[r \left(1 + \sum_{n=1}^{\infty} \mu_{2n} \right) - (q - r) \sum_{n=1}^{\infty} \lambda_{2n-1} \right] / \Omega, \\ q_0 &= \left[(q - r) \left(1 + \sum_{n=1}^{\infty} \lambda_{2n} \right) - r \sum_{n=1}^{\infty} \mu_{2n-1} \right] / \Omega, \end{aligned} \quad (7)$$

where Ω is a constant for given values of R , a_r , and a_q ,

$$\Omega = 1 + \sum_{n=1}^{\infty} \left[\mu_{2n} + \lambda_{2n} + \sum_{i=1}^{\infty} (\mu_{2n} \lambda_{2i} - \mu_{2n-1} \lambda_{2i-1}) \right]. \quad (8)$$

The electric field on an axis x connecting the sphere centers, $E_x = E_x(r, q - r)$, is zero inside the metal spheres and given by the contributions from the image charges

$$E_x = \sum_{n=0}^{\infty} \left[\frac{r_n (x - d_n^r)}{|x - d_n^r|^3} + \frac{q_n (x - d_n^q)}{|x - d_n^q|^3} \right] \quad (9)$$

for $x < -a_r$, $a_r < x < R - a_q$, and $x > R + a_q$. The electric potential $\Phi = \Phi(r, q - r)$ at a point x between the spheres is thus

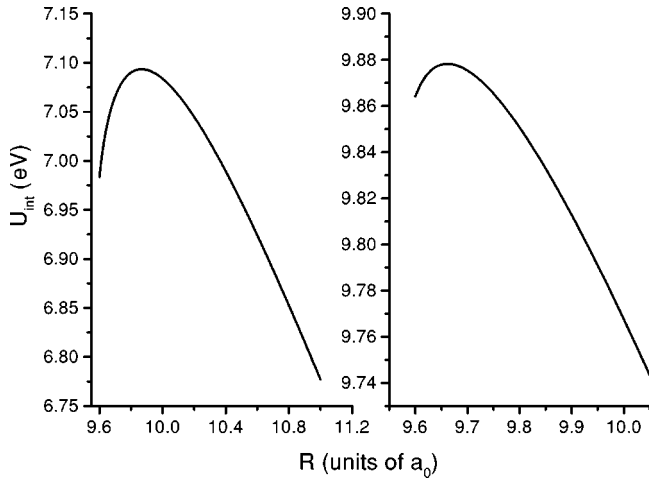


FIG. 3. The interaction energies $U_{int}(R)$ for two charged spheres with radii $a_q=7.2 a_0$ and $a_r=2.3 a_0$ as functions of the center-center distances R . The final charges are $q-r=3$ and $r=1$ (left figure); $q-r=4$ and $r=1$ (right figure). These parameters are chosen for a schematic illustration of the interactions $C_{58}^{3+}-C_2^+$ and $C_{58}^{4+}-C_2^+$, respectively. Note that $U_{int}(R=\infty)=0$ in both cases.

$$\Phi = \sum_{n=0}^{\infty} \left[\frac{r_n}{|x-d_n^r|} + \frac{q_n}{|d_n^q-x|} \right]. \quad (10)$$

This expression immediately gives the total potential energy for two charged spheres as a function of the center-center distance $R > a_q + a_r$ as

$$U_{tot}(R) = U_{int}(R) + U_{\infty}, \quad (11)$$

where U_{int} is the sphere-sphere interaction energy

$$U_{int}(R) = \frac{1}{2} \left[(q-r)\Phi^{x=R-a_q} - \frac{(q-r)^2}{a_q} + r\Phi^{x=a_r} - \frac{r^2}{a_r} \right] \quad (12)$$

and $\Phi^{x=R-a_q}$ and $\Phi^{x=a_r}$ are the electrostatic potentials due to the interaction of the projectile and target spheres, respectively. The additional contribution U_{∞} to the total energy U_{tot} is the energy required to remove $q-r$ and r electrons from the projectile (A) and target (B) spheres when they are at infinite center-center distance

$$U_{\infty} = \sum_{k=1}^{q-r} I_k^A + \sum_{k=1}^r I_k^B. \quad (13)$$

Here, I_k is the binding energy of the k th electron to a sphere of radius a_k ,

$$I_k = W + (k-1/2)/a_k, \quad (14)$$

when $R=\infty$ and W is the bulk work function [30–32].

In Fig. 3, we show two examples for $U_{int}(R)$ with parameters typical for the interactions $C_{58}^{3+}-C_2^+$ and $C_{58}^{4+}-C_2^+$, respectively. These potentials may then be used to deduce fusion barriers and typical kinetic-energy releases in the fis-

sion of C_{60}^{4+} and C_{60}^{5+} . The shapes of the barriers are due to the strong polarizations of both spheres (as given by the two infinite series of image charges) at small distances, while the pure Coulomb term $(q-r)r/R$ dominates at large separations. Using Eq. (12), we arrive at the same result as Näher *et al.* [24] for the shapes of the interaction potentials for sodium metal clusters.

B. A point charge and two metal spheres

In this section, we will extend the ideas presented in the preceding section (and in Ref. [24]) and derive an expression for the electrostatic potential for an electron moving from the target sphere to the projectile, and in the following section we will deduce critical distances for over-the-barrier electron transfer. The electron is assumed to be at a position x on an axis through the centers of the two spheres. By first moving the active target electron to $x=\infty$, the net target charge increases from r to $r+1$ and the sphere center charges are then given by [cf. Eq. (7)]

$$r_0 = \left[(r+1) \left(1 + \sum_{n=1}^{\infty} \mu_{2n} \right) - (q-r) \sum_{n=1}^{\infty} \lambda_{2n-1} \right] / \Omega, \quad (15)$$

$$q_0 = \left[(q-r) \left(1 + \sum_{n=1}^{\infty} \lambda_{2n} \right) - (r+1) \sum_{n=1}^{\infty} \mu_{2n-1} \right] / \Omega,$$

where $r_0 = r_0(q-r, r+1)$, $q_0 = q_0(q-r, r+1)$, and Ω is given by Eq. (8). Moving the active electron to a position x between the spheres leads to changes in the polarizations of both spheres as described by additional infinite sets of image charges at

$$x_1^r = a_r^2/x,$$

$$x_1^q = R - a_q^2/(R-x) \quad (16)$$

and

$$x_{n+1}^r = a_r^2/x_n^q,$$

$$x_{n+1}^q = R - a_q^2/(R-x_n^r) \quad (17)$$

for $n \geq 1$. The corresponding absolute magnitudes are

$$r_1^e = a_r/x,$$

$$q_1^e = a_q/(R-x) \quad (18)$$

and

$$r_{n+1}^e = -q_n^e a_r / x_n^q,$$

$$q_{n+1}^e = -r_n^e a_q / (R-x_n^r) \quad (19)$$

for $n \geq 1$. The sums of the image charges r_n^e and q_n^e are

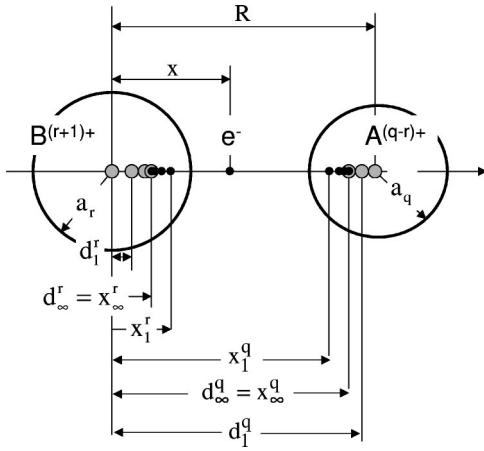


FIG. 4. Image charges induced in the presence of an electron between the spheres d_n^r (gray circles), d_n^q (gray circles), x_n^r (black circles), and x_n^q (black circles).

$$r^e = \sum_{n=1}^{\infty} r_n^e,$$

$$q^e = \sum_{n=1}^{\infty} q_n^e, \quad (20)$$

and since the net charges $r+1$ and $q-r$ must be left intact, charges $-r^e$ and $-q^e$ must be added to the target and projectile spheres, respectively. In analogy with Eq. (7), the magnitudes of the center charges will be shifted by

$$\delta r_0^e = \left[-r^e \left(1 + \sum_{n=1}^{\infty} \mu_{2n} \right) + q^e \sum_{n=1}^{\infty} \lambda_{2n-1} \right] / \Omega,$$

$$\delta q_0^e = \left[-q^e \left(1 + \sum_{n=1}^{\infty} \lambda_{2n} \right) + r^e \sum_{n=1}^{\infty} \mu_{2n-1} \right] / \Omega. \quad (21)$$

The image charges at d_n^r and d_n^q will then also be shifted by

$$\delta r_{2n-1}^e = \lambda_{2n-1} \delta q_0^e,$$

$$\delta r_{2n}^e = \lambda_{2n} \delta r_0^e,$$

$$\delta q_{2n-1}^e = \mu_{2n-1} \delta r_0^e,$$

$$\delta q_{2n}^e = \mu_{2n} \delta q_0^e. \quad (22)$$

The total center charges thus become $r_0 + \delta r_0^e$ and $q_0 + \delta q_0^e$ for the case of an electron positioned at x between target and projectile spheres with total charges $r+1$ and $q-r$, respectively. In Fig. 4, we show the positions of the image charges given by Eq. (1) and (17) schematically. An argument in analogy with the one in the preceding section shows that x_∞^r and x_∞^q are described by expressions of the same form as those for d_∞^r and d_∞^q [Eq. (2)]. As indicated in Fig. 4, the two series (x_n and d_n) converge to the same positions in the spheres but from opposite directions. In Fig. 5, we display the positions of the target image charges with sphere radii,

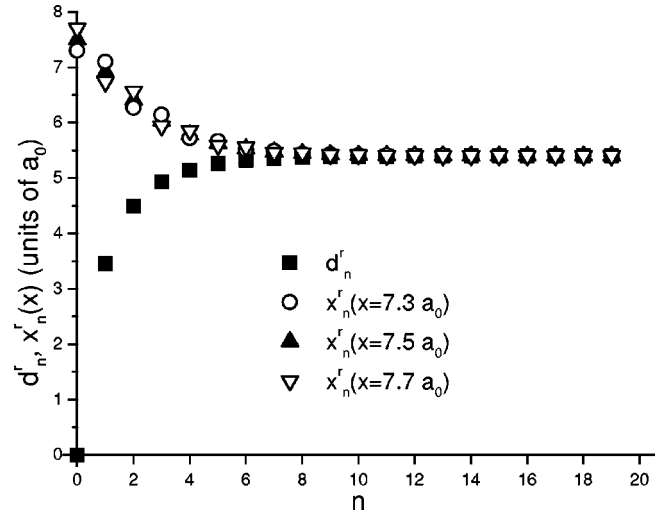


FIG. 5. The positions of the target image charges for different electron positions x . The center-center distance is $R = 15 a_0$ and the target and projectile radii are $a_r = a_q = 7.2 a_0$.

$a_q = a_r = 7.2 a_0$, and three different positions x for the electron. Note that x_n^r , unlike d_n^r , depend on x but that d_∞^r and x_∞^r approach a common constant value regardless of the value of x . Outside the spheres, all image charges contribute to the electric field $E_x = E_x(r+1, q-r)$, yielding

$$E_x = \sum_{n=0}^{\infty} \left[\frac{r_n(x-d_n^r)}{|x-d_n^r|^3} + \frac{q_n(x-d_n^q)}{|x-d_n^q|^3} \right] + \sum_{n=1}^{\infty} \left[\frac{r_n^e(x-x_n^r)}{|x-x_n^r|^3} + \frac{q_n^e(x-x_n^q)}{|x-x_n^q|^3} \right] + \sum_{n=0}^{\infty} \left[\frac{\delta r_n^e(x-d_n^r)}{|x-d_n^r|^3} + \frac{\delta q_n^e(x-d_n^q)}{|x-d_n^q|^3} \right] \quad (23)$$

at the position x of the electron. The first sum gives the contribution to the electric field when the electron is at infinity and is formally identical to Eq. (9). The second and third sums are the contributions due to the presence of the electron. The potential that the electron experiences is zero at infinity and its value at a position x is extracted from the work (W_e) required to move the electron from infinity to x ,

$$\Phi = \frac{W_e}{q_e} = -\frac{1}{q_e} \int_{\infty}^x F_x dx = -\int_{\infty}^x E_x dx, \quad (24)$$

where $F_x = q_e E_x$ is the force acting on the electron and $q_e = -1$ a.u. is the charge of the electron. Note that r_n^e , q_n^e , x_n^r , x_n^q , δr_n^e , and δq_n^e depend on x , which makes the integration of the second and third sums in Eq. (23) rather involved. Numerical calculations, however, converge to the following analytical expression for the potential $\Phi = \Phi(r+1, q-r)$, which the electron experiences at an arbitrary position x between the spheres:

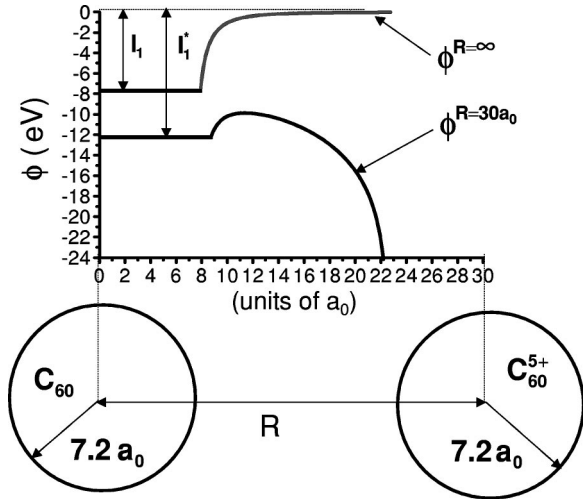


FIG. 6. The potential $\Phi(x)$ seen by an electron moving from the target to the projectile C_{60} molecule ($q-r=5, r=0$). The maximum of the potential barrier is higher than the Stark-shifted ionization potential (I_1^*). Thus the over-the-barrier condition is not fulfilled and the electron is therefore still bound to the target.

$$\Phi = -\sum_{n=0}^{\infty} \left[\frac{r_n}{|x-d_n^r|} + \frac{q_n}{|d_n^q-x|} \right] - \frac{1}{2} \sum_{n=1}^{\infty} \left[\frac{r_n^e}{|x-x_n^r|} + \frac{q_n^e}{|x_n^q-x|} \right] - \frac{1}{2} \sum_{n=0}^{\infty} \left[\frac{\delta r_n^e}{|x-d_n^r|} + \frac{\delta q_n^e}{|d_n^q-x|} \right]. \quad (25)$$

which includes the full multipole expansions of all polarization effects.

C. Charge transfer between the spheres

The critical distances (R_{r+1}) at which an electron is transferred from the target to the projectile are given by the over-the-barrier conditions. These are fulfilled when the maxima of the potentials Φ in Eq. (25) become lower than the corresponding Stark-shifted target ionization potential I_{r+1}^* ,

$$\Phi^{max} \leq I_{r+1}^* = I_{r+1} + \Phi_{r,q-r}^{x=a_r} - r/a_r. \quad (26)$$

where $\Phi_{r,q-r}^{x=a_r} - r/a_r$ is the Stark shift that the electron experiences at the target [Eq. (10)] and I_{r+1} is the binding energy of the $(r+1)$ th electron to the target [Eq. (14)].

The potential $\Phi(x)$ [Eq. (25)] seen by an electron at x between two C_{60} molecules ($q-r=5, r=0$) modeled as metal spheres is shown in Fig. 6. Here, we assume that the model sphere radius is independent of the sphere charge and use a linear fit of the experimental sequence of ionization potentials [33] to Eq. (14) (as a function of k) yielding $a_r = a_q = 7.2 a_0$ and $W = 5.7$ eV. The Stark-shift term is zero at infinite center-center distance $R = \infty$. For decreasing R , the potential barrier decreases and the binding energy of the first active electron on the target is down shifted to I_1^* . The $R = 30 a_0$ case shown in Fig. 6 corresponds to a situation where the first electron transfer is not possible according to

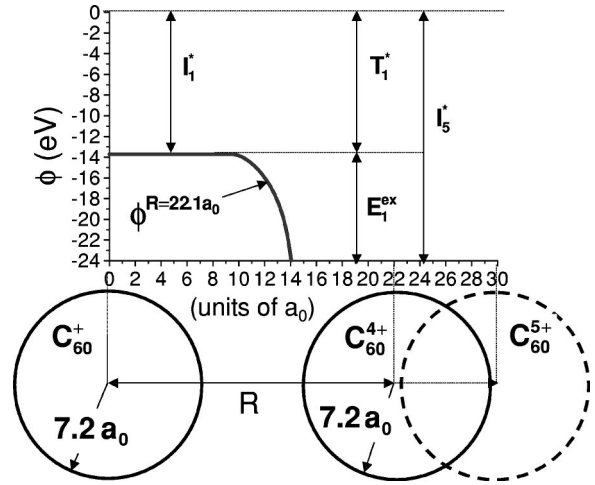


FIG. 7. The potential barrier $\Phi(x)$ between two C_{60} molecules at the first critical distance $R_1 = 22.1 a_0$. The Q value and the excitation energy can be derived from the resonance condition $\{I_1^* = T_1^*$ [Eq. (27)] and the Stark-shifted ionization potential of the projectile (I_5^*).

the over-the-barrier condition. This condition is, however, fulfilled when the projectile is closer to the target ($R = 22.1 a_0$), as indicated in Fig. 7. We assume that there is a resonant state on the projectile sphere at this moment (quasicontinuum approximation). The resonance condition ($I_1^* = T_1^*$) is then given by

$$I_1 + \Phi_{r=0,q-r=5}^{x=a_r} = T_1 + \Phi_{r=1,q-r=4}^{x=R_1-a_q} - (q-r)/a_q, \quad (27)$$

where the left-hand side ($q-r=5$) is the Stark-shifted binding energy of the electron located to the target at the critical center-center distance, R_1 . The right-hand side ($q-r=4$) is the corresponding energy when the electron is localized to the projectile. When the spheres separate again to infinite center-center distances after the collision, the Stark-shift terms tend to zero. The Q value for one-electron transfer from the target to the projectile is defined as the difference in binding energies to the projectile and the target, $Q_1 = T_1 - I_1$. According to the resonance condition [Eq. (27)] this equals the difference in Stark shifts at the critical distance R_1 [23]. The excitation energy of the transferred electron in single-electron capture is the difference in the Stark-shifted ionization potentials when the electron is in the target and projectile ground states, respectively, $E_1^{ex} = I_5^*(R_1) - I_1^*(R_1)$.

The Q -value for transfer of r electrons is

$$Q_r = \sum_{k=1}^r (T_k - I_k), \quad (28)$$

while the total excitation energy of r transferred electron is given by

$$E_{tot}^{ex} = \sum_{k=1}^r [I_{q-k+1}^*(R_k) - I_k^*(R_k)]. \quad (29)$$

D. Relations to ion-sphere and ion-atom OBM models

For a point-formed projectile ($a_q=0$) and a spherical target ($a_r=7.2 a_0$), the only nonvanishing charges in Eqs. (3), (7), (15), (18), (19), (21), and (22) are the center charges $r_0=r-r_1+1$, $q_0=q-r$, and $\delta r_0=-r_1^e$ and the image charges r_1 and r_1^e , giving only two dipole contributions to the target polarization. The potential in Eq. (25) is then given by

$$\Phi_{a_q=0}(x) = -\frac{q-r}{R-x} + \frac{a_r(q-r)}{Rx-a_r^2} - \frac{a_r(q-r)}{Rx} - \frac{r+1}{x} + \frac{1}{2} \left(\frac{a_r}{x^2} - \frac{a_r}{x^2-a_r^2} \right) \quad (30)$$

and the resonance condition corresponding to Eq. (26) becomes

$$I_{r+1} + (q-r)/R = \Phi_{a_q=0}^{max}. \quad (31)$$

This is identical to the results of the over-the-barrier model for atomic ions and (spherical) clusters [16]. When, in addition, the target radius is set to zero (i.e., $a_r=a_q=0$), the only remaining charges are of course only the net charges $r_0=r+1$ and $q_0=q-r$. The potential and resonance condition are then

$$\Phi_{a_r=a_q=0}(x) = -(q-r)/(R-x) - (r+1)/x \quad (32)$$

and

$$I_{r+1} + (q-r)/R = \Phi_{a_r=a_q=0}^{max}, \quad (33)$$

respectively. Here the critical distances are obtained analytically as

$$R_{r+1} = [2(q-r)^{1/2}(r+1)^{1/2} + (r+1)]/I_{r+1}, \quad (34)$$

which is equivalent to the expression given in the over-the-barrier model for atomic ions and atoms [2].

III. RESULTS AND DISCUSSION

A. Comparisons with TDLDA and Vlasov calculations for Ar^{8+} - Na_{40} collisions

In Fig. 8, we show comparisons between different calculations of the final cluster charge in Ar^{8+} - Na_{40} collisions as a function of the impact parameter. The results based on the TDLDA, which treat the electronic response of a sharply edged jellium target in a fully quantum-mechanical way, were obtained with a target radius of $a_r=13.7$ a.u. [7,9]. The left figure shows results for 80 keV (relative velocity $0.3v_0$), while the right one gives results for 320 keV ($0.6v_0$). As can be seen in Fig. 8 these results differ little from those obtained by solving the Vlasov equation, which is the semiclassical counterpart of the TDLDA [9]. In the two figures we also show the final target charge state as a function of impact parameter according to the present *static* classical OBM using the same target sphere radius ($a_r=13.7$ a.u.). The sim-

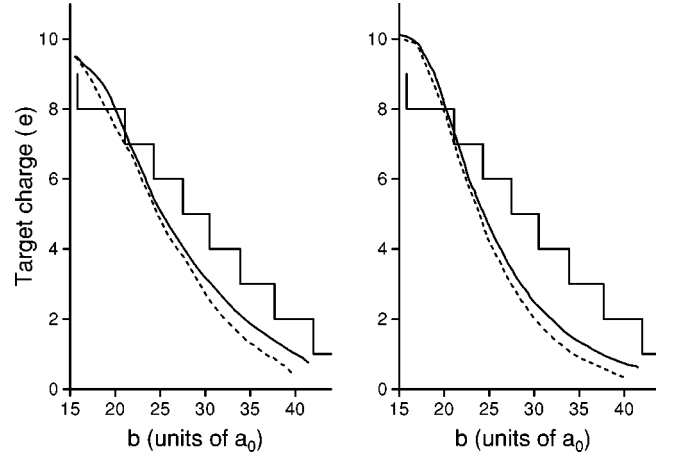


FIG. 8. The number of transferred electrons (the target cluster charge state) as functions of the impact parameter b in Ar^{8+} - Na_{40} collisions at 80 keV (left) and 320 keV (right) using the TDLDA (full curves) and Vlasov (dashed curves) methods. The present static OBM results, for which the resonance condition is ignored and the numbers of electrons located at the target are taken to be discrete, are also shown as the staircases.

plified assumption of this model is that electrons will move over the barrier to the projectile as soon as the barrier becomes sufficiently low for such a transition to become classically allowed. This means that the resonance requirement is ignored and in effect we assume a quasicontinuum of projectile capture states. The static OBM results are thus upper bounds to the results that one would have obtained if the quantum nature of the projectile capture state energies would have been invoked. This is a customary approximation in OBM's [2,11,16] and its justification is that capture proceeds to highly excited states for which the densities of states are high, which is also the case when clusters are involved (see e.g., Ref. [23]). The target charging in discrete steps is of course a consequence of the fact that the charge is not treated as a continuous variable as in the TDLDA and Vlasov calculations [9].

It is clear from the comparison between the left and right parts of Fig. 8 that the *static* OBM becomes a better approximation as the collision velocity decreases. This is connected to the fact that the electrons that moves in the cluster at characteristic velocities will have more time to make the transition to the projectile. From the improvement in the agreement when decreasing the collision velocity from 0.6 to $0.3 v_0$, we expect that the *static* OBM will give results on the target charging close to those obtained with the full TDLDA (or Vlasov) at significantly lower energies. How low the collision velocity has to be in order to fulfill this requirement does of course depend on the target. This has been demonstrated by Plagne and Guet [8], who made Vlasov calculations for Ar^{8+} - Na_{196} at $0.4 v_0$ giving much lower target charges than the static OBM. This is due to the much lower ionization potentials, and thus lower characteristic velocities) of the larger cluster [see Eq. (14)]. Note that the overcharging of the target at small b —the target charge exceeds the incident projectile charge—which was observed in TDLDA and Vlasov calculations [7–9] also appears in the

present static OBM, which does not consider electron emission during the collision. From the comparison in this section we conclude that the static OBM is a reasonable approximation for the very slow, ion-cluster, cluster-cluster, and sphere-sphere collisions ($v < 0.1 v_0$) which will be considered in the following comparisons with various experimental results.

B. Relative charge-exchange cross sections in C_{60}^{q+} - C_{60} and C^{q+} - C_{60} collisions

Recently, members of the present collaboration [25] reported on an experimental investigation of charge transfer in C^{q+} - C_{60} and C_{60}^{q+} - C_{60} collisions at $0.06\sqrt{q} v_0$ and $0.01\sqrt{q} v_0$, respectively. The projectile charge state q ranged from $q=1$ to $q=5$ but whereas C_{60} was ionized up to $r_{max}=q$ for atomic projectiles, the corresponding maximum target charge was limited to $r_{max}=\text{Int}[(q+1)/2]$, for the fullerene projectiles. In the latter case, no fragmentation of the target was observed Ref. [25]. As argued in Ref. [25], the empirical result $r_{max}=\text{Int}[(q+1)/2]$ can be understood by modeling the molecules as conducting spheres that fragment at certain small, but nonzero, surface-surface distances. For even charged projectiles, the charges will be equally divided on the two spheres, while for odd q , the last charge may or may not end up on the target after separation. In the case of an atomic projectile, such as C^{q+} , it has been shown before that the static over-the-barrier model is able to account for full neutralization of the projectile at distances well outside the surface of a model sphere C_{60} target [23].

Here, we are aiming at a quantitative comparison between experimental and model relative charge state fractions, which are defined as σ_r/σ_{tot} where σ_r is the cross section for removing r electrons from the target without fragmentation and σ_{tot} is the corresponding total *nonfragmenting* ionization cross section. In the sphere-sphere case, we define the model cross sections for *even* q as

$$\sigma_r = \pi(R_r^2 - R_{r+1}^2) \quad (35)$$

when $r < r_{max}$ and

$$\sigma_r = \pi(R_{r_{max}}^2 - b_{max}^2) \quad (36)$$

when $r = r_{max}$. Here, b_{max} is defined semiempirically (i.e., from comparisons with the measurements) as the maximum impact parameter for fragmentation of the target (see below). The corresponding definitions for *odd* q are

$$\sigma_r = \frac{\pi}{2}(R_{r_{max}}^2 - b_{max}^2) \quad (37)$$

when $r = r_{max}$ and

$$\sigma_r = \pi(R_r^2 - R_{r_{max}}^2) + \frac{\pi}{2}(R_{r_{max}}^2 - b_{max}^2) \quad (38)$$

when $r = r_{max} - 1$. For lower r we use Eq. (35). The total model nonfragmentation ionization cross section for odd and even q is

TABLE I. Critical distances for electron transfer in C_{60}^{q+} - C_{60} collisions.

q	2	3	4	5
R_1	18.5 a_0	19.5 a_0	20.8 a_0	22.1 a_0
R_2		17.7 a_0	18.4 a_0	19.3 a_0
R_3				17.7 a_0

$$\sigma_{tot} = \sum_{r=1}^{r_{max}} \sigma_r = \pi(R_1^2 - b_{max}^2). \quad (39)$$

In the case of atomic projectiles, we use Eqs. (35), (36), and (39) for odd and even q . The critical over-the-barrier distances for charge transfer in the sphere-sphere (C_{60}^{q+} - C_{60}) collisions with $a_q = a_r = 7.2 a_0$ and in point charge-sphere (C^{q+} - C_{60}) collisions with $a_q = 0$ and $a_r = 7.2 a_0$, are given in Tables I and II, respectively. The b_{max} values are then defined semiempirically using the model critical radii and the measured values for $\sigma_{r_{max}}/\sigma_{tot}$ for $q=5$ yielding the results $b_{max} = 17.2 a_0$ ($r_{max}=3$) and $b_{max} = 11.4 a_0$ ($r_{max}=5$) for C_{60}^{q+} and the C^{q+} projectiles, respectively. The comparison between the model and experimental [25] results are shown in Fig. 9.

C. Excitation energies in C_{60}^{4+} - C_{60} collisions

Figure 10 shows C_{60} recoil ion spectra measured in coincidence with final intact fullerene projectiles C_{60}^{3+} (upper part of Fig. 10) and C_{60}^{2+} (lower part of Fig. 10), resulting from 10-keV C_{60}^{4+} - C_{60} collisions [26]. Note that there are no doubly charged recoils in the upper spectrum, that is the transfer ionization process of the type often dominant in slow collisions and mediated via an intermediate doubly excited projectile state [$C_{60}^{4+} + C_{60} \rightarrow (C_{60}^{2+})^{**} + C_{60}^{2+} \rightarrow C_{60}^{3+} + C_{60}^{2+} + e^-$] is strongly suppressed. True double-electron capture ($C_{60}^{4+} + C_{60} \rightarrow C_{60}^{2+} + C_{60}^{2+}$) is, however, seen as a strong peak in the target spectrum of Fig. 10 (lower part). The suppression of the transfer ionization process is due to the relatively low excitation energy of C_{60}^{2+} formed in C_{60}^{4+} - C_{60} collisions. The reason for this is clearly exposed by the present over-the-barrier model. According to this model the first electron is captured to the projectile in an excited state. The left part of Fig. 11 is a schematic display of the calculated excitation ($E_1^{ex} = 7$ eV), and binding ($T_1 = 12$ eV) energies (which of course are given for $R = \infty$),

TABLE II. Critical distances for electron transfer in C^{q+} - C_{60} collisions.

q	2	3	4	5
R_1	16.6 a_0	18.7 a_0	20.5 a_0	22.0 a_0
R_2	13.2 a_0	15.5 a_0	17.3 a_0	18.9 a_0
R_3		12.7 a_0	14.8 a_0	16.4 a_0
R_4			12.3 a_0	14.2 a_0
R_5				11.9 a_0

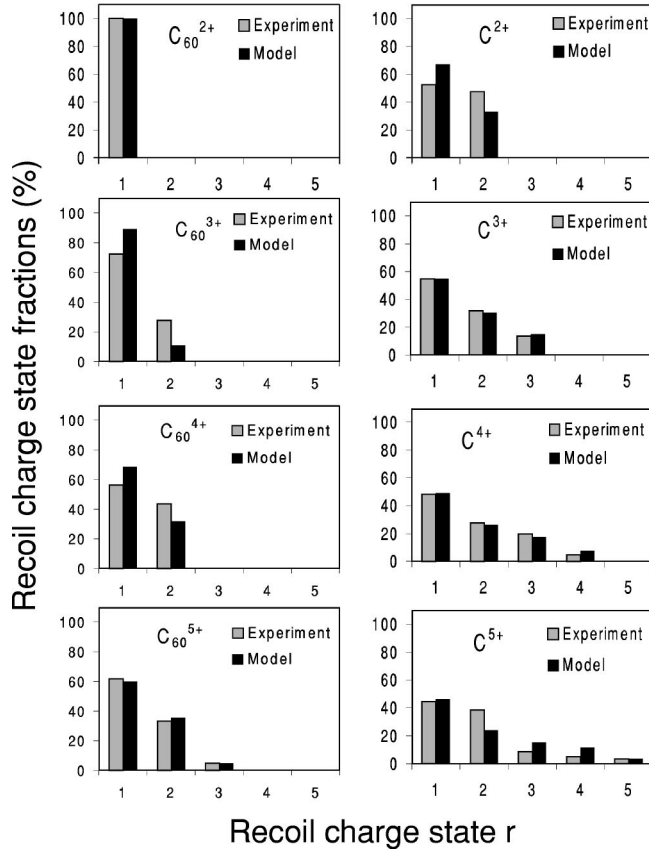


FIG. 9. Model and experimental recoil charge state fractions for C_{60}^{q+} - C_{60} and C^{q+} - C_{60} collisions. Only intact C_{60} target ions are included in the fractions.

and the energy required to ionize the isolated C_{60}^{3+} [$I_4 = 19$ eV; calculated from Eq. (14)]. In the right part of Fig. 11 the calculated total excitation energy $\{E_{tot}^{ex} = 9$ eV [Eq. (29)] $\}$ of C_{60}^{2+} is compared to the ionization energy ($I_3 = 15$ eV). Thus the model suggests that transfer ionization channel is prohibited for energetic reasons, which is in accordance with the experimental observations [26].

D. Projectile electron loss in Lys- H_9^{9+} - O_2 collisions

Recently, Hvelplund *et al.* [27] reported on measurements of *electron loss* from highly protonated lysozyme ions Lys- H_9^{9+} (ionization potential 11 eV [27]—giving target electron velocities around $0.9 v_0$), colliding with O_2 at $0.01 v_0$. At a first glance it is quite surprising that such a highly charged projectile loses an electron in a collision with a neutral molecule. This observation contrasts strongly to the ones made for collisions involving highly charged atomic and (smaller) molecular ions where electron capture always is dominant. As already pointed out by Hvelplund *et al.* [27], there are two important features of the Lys- H_9^{9+} - O_2 collision system, which gives clues to how to understand the electron-loss process. First, Lys- H_9^{9+} is a very large (and roughly spherical) molecule with a radius of $a_q = 37.8 a_0$ [27], which indicates that polarization effects are important. Second, the O_2 -molecule has a large electron affinity which

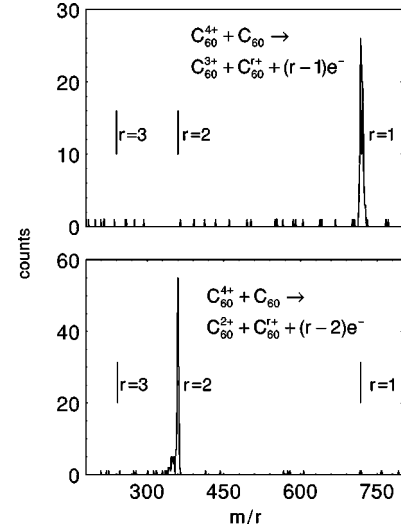


FIG. 10. Mass-to-charge (m/r) spectra in atomic units for 10-keV C_{60}^{4+} - C_{60} collisions. The spectra are measured in coincidence with C_{60}^{3+} product ions (upper figure) and C_{60}^{2+} product ions (lower figure).

makes it possible to capture an electron to the neutral molecule as was recently verified experimentally by Tomita *et al.* [34]. The total Lys- H_9^{9+} beam attenuation cross section, which is the sum of the nonfragmenting electron loss and the fragmentation cross sections, was measured to be $(5.5 \pm 0.5) \times 10^3 a_0^2$ [27].

Here, we use the present model for electron transfer between two spheres using $a_q = 37.8 a_0$ and $a_r = 2.2 a_0$, the latter deduced from $a_r = \alpha^{1/3}$ and the dipole polarizability of O_2 $\alpha = 10.7 a_0^3$ [35]. We calculate the critical distance at which the potential barrier between the spheres becomes low enough for an electron to be removed from the projectile ($q=9$) with $I_{10} = 11$ eV [27] by a neutral target ($r=0$). This critical distance ($R_1 = 43.3 a_0$) gives a total model cross section for electron loss (including also fragmentation processes) of $5.9 \times 10^3 a_0^2$, which agrees with the measured attenuation cross section.

The pure nonfragmenting electron-loss cross section was measured to be $360 a_0^2$ [27], which is only a small fraction of the total attenuation cross section. Here, we use Eqs. (11) and (13) to calculate the curve crossing between the sphere-

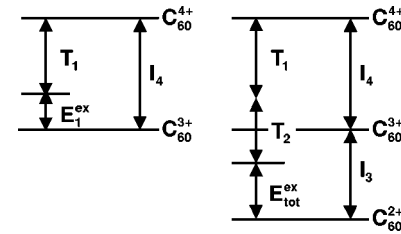


FIG. 11. The total model binding T_1 and $(T_1 + T_2)$ and excitation energies E_1^{ex} and E_{tot}^{ex} for $C_{60}^{4+} + C_{60} \rightarrow C_{60}^{3+} + C_{60}^{+}$ and $C_{60}^{4+} + C_{60} \rightarrow C_{60}^{2+} + C_{60}^{2+}$ collisions, respectively. Note that the total excitation energy E_{tot}^{ex} , is smaller than the ionization energy of C_{60}^{2+} ($I_3 = 15$ eV).

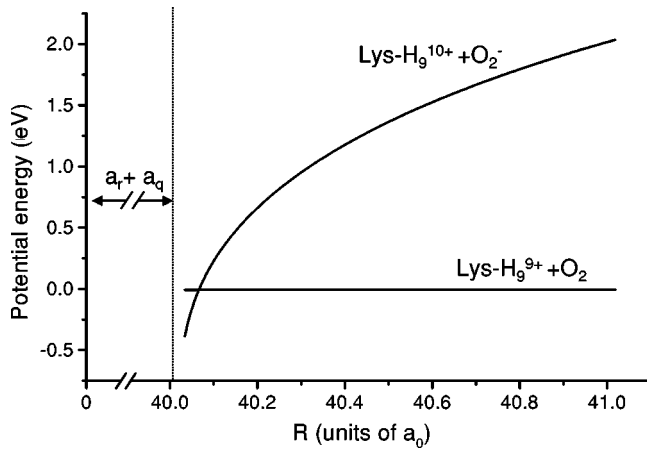


FIG. 12. The potential energy curves as a function of center-center distance when an electron is localized to the projectile ($\text{Lys-H}_9^{9+} + \text{O}_2$) and the target ($\text{Lys-H}_9^{10+} + \text{O}_2^-$), respectively. The curve crossing lies just outside the distance for which the target surface touches the projectile surface ($a_r + a_q = 40 a_0$), but inside the critical distance ($R_1 = 43.3 a_0$).

sphere potentials with the active electron localized to either the target (O_2) or projectile (Lys-H_9^{9+}) spheres. The crossing distance lies inside the critical distance ($R_1 = 43.3 a_0$) for electron removal from the highly charged projectile sphere as can be seen in Fig. 12. At slightly smaller distances ($< 37.8 a_0 + 2.2 a_0$) fragmentation processes become very strong due to elastic atom-atom collisions.

IV. CONCLUSIONS

In this work, we have presented a *static* classical over-the-barrier model for sequential multiple-electron transfer between two metal spheres. The model gives the total and absolute cross sections for transfer of r electrons from the target to the projectile and the corresponding Q values and total excitation energies. By letting the projectile sphere radius approach zero the present model reduces to the over-the-barrier model for (atomic) ion-metal sphere collisions [16], while we arrive at the corresponding ion-atom model [2] when both radii tend to zero. On the basis of comparisons with full quantum-mechanical TDLDA calculations for the electronic response of a Na_{40} cluster (jellium model) colliding with slow Ar^{8+} ions, we conclude that the static OBM may be used for moderately sized clusters in collisions with

velocities below $0.1 v_0$. The relative recoil charge state fractions for such $\text{C}^{q+} - \text{C}_{60}$ and $\text{C}_{60}^{q+} - \text{C}_{60}$ collisions have been shown to be in good agreement with similar recent experimental results [25]. Further, the model accounts for the observed complete suppression of transfer ionization in $\text{C}_{60}^{4+} - \text{C}_{60}$ collisions at $0.02 v_0$ [26] as the calculated total excitation energy of the formed doubly excited projectile state is smaller than the third ionization potential of C_{60} . We have also shown that the electron loss and dissociation cross section in highly protonated Lysozyme-oxygen ($\text{Lys-H}_9^{9+} - \text{O}_2$) collisions at $0.01 v_0$ are reproduced by the present calculations, which also shows that O_2^- is formed through a curve crossing inside the critical distance for electron transfer but outside the radius for fragmentation. The main advantage with the present model is its great simplicity and the fact that it is able to provide first estimates of important observables in, e.g., cluster-cluster collisions—such as the very recent example of Ubiquitin- C_{60} collisions [37]. Its usefulness at higher collision velocities is more limited, but there are—as we have shown in this work—many applications in which it might be extremely useful at low v .

The work to incorporate the influences from over-the-barrier electron transfer processes in the descriptions of fragmentation of multiply charged metal clusters is in progress. We also note that electron transfer processes involving one or several charged objects might be important for the understanding of charge balance in dilute astrophysical plasmas containing, e.g., spherical conducting dust particles [36]. A further possible extension of the present model with applications in chemistry would be to consider electron transfer between dielectric spheres in solutions, with obvious applications for studies in biochemistry concerning, e.g., long-range forces between overcharged macroions in solutions [38]. In the near future, the model will be used for comparisons with experimental results on fragmentation and fusion of metal clusters taking charge transfer during these processes into account.

ACKNOWLEDGMENTS

This work was supported by the Swedish Research Council under Contract No. 621-2001-2226 and the Swedish Foundation for International Cooperation in Research and Higher Education (STINT) at the Manne Siegbahn Laboratory. The collaboration was organized within the framework of the European network LEIF Grant No. (HPRI-CT-1999-40012).

-
- [1] H. Ryufuku, K. Sasaki, and T. Watanabe, *Phys. Rev. A* **21**, 745 (1980).
 - [2] A. Bárány, G. Astner, H. Cederquist, H. Danared, S. Huldt, P. Hvelplund, A. Johnson, H. Knudsen, L. Liljeby, and K.-G. Rensfelt, *Nucl. Instrum. Methods Phys. Res. B* **9**, 397 (1985).
 - [3] A. Niehaus, *J. Phys. B* **19**, 2925 (1986).
 - [4] J. Burgdörfer, P. Lerner, and F.W. Meyer, *Phys. Rev. A* **44**, 5674 (1991).
 - [5] L. Hägg, C.O. Reinhold, and J. Burgdörfer, *Phys. Rev. A* **55**, 2097 (1997).
 - [6] U. Thumm, A. Bárány, H. Cederquist, L. Hägg, and C.J. Satterlind, *Phys. Rev. A* **56**, 4799 (1997).
 - [7] K. Yabana, T. Tazawa, Y. Abe, and P. Bozek, *Phys. Rev. A* **57**, R3165 (1998).
 - [8] L. Plagne and C. Guet, *Phys. Rev. A* **59**, 4461 (1999).
 - [9] L. Plagne, J. Daligault, K. Yabana, T. Tazawa, Y. Abe, and C.

- Guert, Phys. Rev. A **61**, 033201 (2000).
- [10] O. Knospé, J. Jellinek, U. Saalmann, and R. Schmidt, Phys. Rev. A **61**, 022715 (2000).
- [11] B. Walch, C.L. Cocke, R. Voelpel, and E. Salzborn, Phys. Rev. Lett. **72**, 1439 (1994).
- [12] H. Shen, P. Hvelplund, D. Mathur, A. Bárány, H. Cederquist, N. Selberg, and D.C. Lorents, Phys. Rev. A **52**, 3847 (1995).
- [13] F. Rohmund and E.E.B. Campbell, Chem. Phys. Lett. **245**, 237 (1995).
- [14] N. Selberg, A. Bárány, C. Biedermann, C.J. Setterlind, H. Cederquist, A. Langereis, M.O. Larsson, A. Wännström, and P. Hvelplund, Phys. Rev. A **53**, 874 (1996).
- [15] B. Walch, U. Thumm, M. Stöckli, C.L. Cocke, and S. Klavikowski, Phys. Rev. A **58**, 1261 (1998).
- [16] H. Cederquist, A. Fardi, K. Haghighat, A. Langereis, H.T. Schmidt, S.H. Schwartz, J.C. Levin, I.A. Sellin, H. Lebius, B. Huber, M.O. Larsson, and P. Hvelplund, Phys. Rev. A **61**, 022712 (2000).
- [17] J.U. Andersen, C. Brink, P. Hvelplund, M.O. Larsson, B. Bech Nielsen, and H. Shen, Phys. Rev. Lett. **77**, 3991 (1996).
- [18] S. Martin, L. Chen, A. Denis, and J. Désesquelles, Phys. Rev. A **59**, 1734 (1999).
- [19] L. Chen, S. Martin, R. Brédy, J. Bernard, and J. Désesquelles, Phys. Rev. A **64**, 031201 (2001).
- [20] O. Hadjar, P. Földi, R. Hoekstra, R. Morgenstern, and T. Schlathölter, Phys. Rev. Lett. **84**, 4076 (2000).
- [21] J. Opitz, H. Lebius, S. Tomita, B.A. Huber, P. Moretto Capelle, D. Bordenave Montesquieu, A. Bordenave Montesquieu, A. Reinkster, U. Werner, H.O. Lutz, A. Niehaus, M. Benndorf, K. Haghighat, H.T. Schmidt, and H. Cederquist, Phys. Rev. A **62**, 022705 (2000).
- [22] A. Bárány and C.J. Setterlind, Nucl. Instrum. Methods Phys. Res. B **98**, 184 (1995).
- [23] A. Langereis, J. Jensen, A. Fardi, A. Haghighat, H.T. Schmidt, S.H. Schwartz, H. Zettergren, and H. Cederquist, Phys. Rev. A **63**, 062725 (2001).
- [24] U. Näher, S. Björnholm, S. Frauendorf, F. Garcias, and C. Guet, Phys. Rep. **285**, 245 (1997).
- [25] H. Cederquist, P. Hvelplund, H. Lebius, H. T Schmidt, S. Tomita, and B.A. Huber, Phys. Rev. A **63**, 025201 (2001).
- [26] H. Lebius, B.A. Huber, S. Tomita, P. Hvelplund, J. Jensen, H. T. Schmidt, H. Zettergren, and H. Cederquist, Phys. Rev. A (submitted).
- [27] P. Hvelplund, S.B. Nielsen, M. Sørensen, J.U. Andersen, and T.J.D. Jørgensen, J. Am. Soc. Mass Spectrom. **12**, 889 (2001).
- [28] J.D. Jackson, *Classical Electrodynamics* (Wiley, New York, 1975).
- [29] H. Cheng, SIAM (Soc. Ind. Appl. Math.) J. Appl. Math. **61**, 1324 (2000).
- [30] W.A. de Heer and P. Milani, Phys. Rev. Lett. **65**, 3356 (1990).
- [31] M. Seidl, K.-H. Meiwes-Broer, and M. Brack, J. Chem. Phys. **95**, 1295 (1991).
- [32] U. Näher, H. Gölich, T. Lange, and T.P. Martin, Phys. Rev. Lett. **68**, 3416 (1992).
- [33] G. Javahery, H. Vincel, S. Pteric, and D.K. Bohme, Chem. Phys. Lett. **204**, 467 (1993).
- [34] S. Tomita, J.S. Forster, P. Hvelplund, and S. Brøndstedt Nielsen, Int. J. Mass. Spectrom. **214**, 57 (2002).
- [35] *CRC Handbook of Chemistry and Physics*, 71st ed., edited by D.R. Lide (CRC Press, Boca Raton, 1990).
- [36] Y.-D. Jung and H. Tawara, Phys. Rev. E **64**, 017401 (2001).
- [37] P. Hvelplund, Bo Liu, S. Brøndstedt Nielsen, S. Tomita, H. Cederquist, J. Jensen, H.T. Schmidt, and H. Zettergren, J. Chem. Phys. (to be published).
- [38] R. Messina, C. Holm, and K. Kremer, Phys. Rev. Lett. **85**, 872 (2000).